ARKIV FÖR FYSIK Band 15 nr 31

Communicated 11 March 1959 by ERIK HULTHÉN and KAI SIEGBAHN

K and *L* energy levels in some fourth and fifth period elements

By CARL NORDLING

With 24 figures in the text

Contents

I Introduction 398
II Experimental conditions 399
  A. Analysis of the electron lines 399
  B. Residual magnetic field 404
III "Absolute" energy calibration 405
  A. Error calculation 406
  B. Residual field correction 408
IV Experimental results 409
  A. The calibration lines 409
    1. Te L_{III}(Cu $K\alpha_1$, Mo $K\alpha_1$) 409
    2. Cu K(Mo $K\alpha_1$, Ag $K\alpha_1$) 411
  B. Binding energies 413
    1. Error estimation 413
    2. Fourth period elements 414
    3. Fifth period elements 418
    4. Work function correction 424
V Discussion of results 425

ABSTRACT

The photo electron method has been applied to a study of the binding energies of *K* and *L* electrons in the elements copper, zinc, gallium, germanium and selenium, and *L* binding energies in the elements rhodium through tellurium. Calibration lines are obtained from "absolute" $B\varrho$-determinations, and the relative accuracy in the subsequent measurements is 2×10^{-5}. The results are given together with representative X-ray data in modified Moseley diagrams. Discontinuities are observed in these curves even as new subshells of the free atom start to build-up. Certain discrepancies seem to exist between the energies obtained with the photo electron method and those determined by the conventional X-ray absorption method.

I. Introduction

The problem of determining binding energies of the inner electronic levels of an atom conventionally has been approached with pure X-ray methods. Generally, the binding of an inner electron has been associated with the energy required for an excitation of the electron to the bottom of the conduction band. Under specific assumptions this can be identified with the energy of the first inflection point of the corresponding absorption edge (1). Consequently, measurements of absorption discontinuities have played a most important role for the determination of electron binding energies. Another method of measuring the same quantity is the study of excitation potentials of X-ray lines (2, 3), in which case the excitation is accomplished by electron impact. However, absorption edges as well as excitation curves have a more or less pronounced structure, and this introduces difficulties in the interpretation of experimental data.

A third method of studying electron binding recently has been developed to such an accuracy as to compete favourably with other methods (4). This is the photo electron method, in which the kinetic energy of the ejected electron itself is measured,

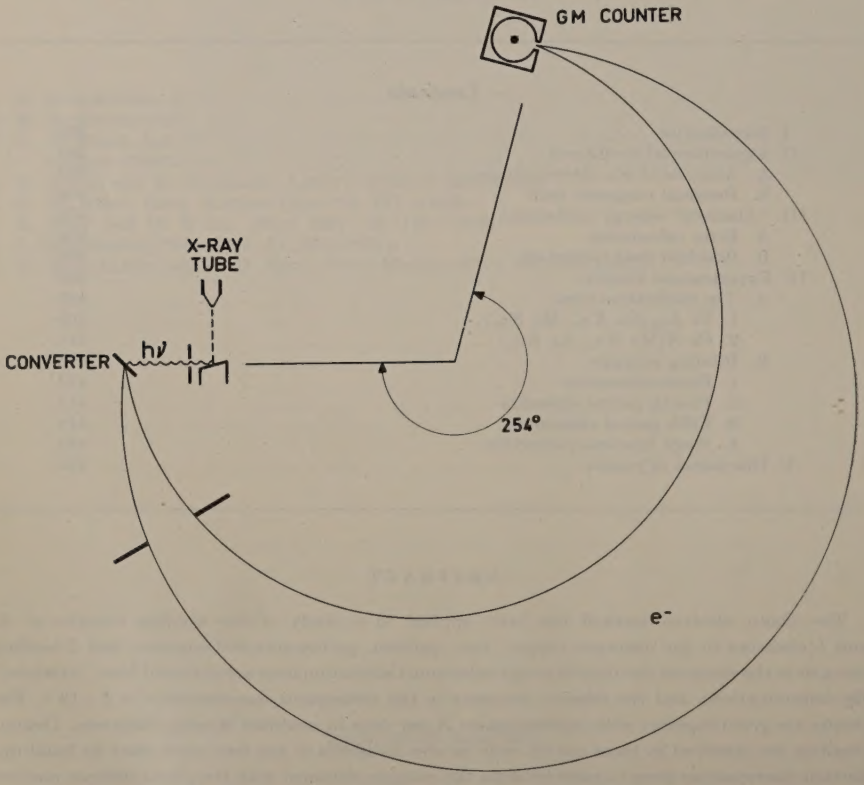

Fig. 1. Schematic drawing of the experimental arrangement.

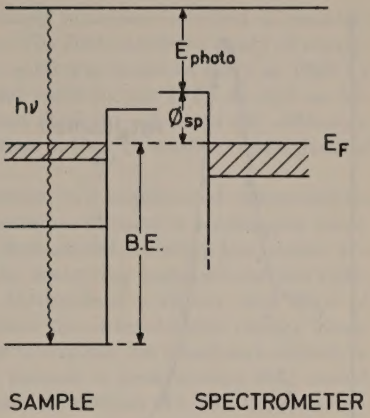

Fig. 2. Energy level diagram of a metallic sample in electrical contact with the spectrometer. As indicated in the figure, the binding energy, B.E., of an electron together with the work function, ϕ_{sp}, of the spectrometer material and the kinetic energy, E_{photo}, of the ejected electron as measured in the spectrometer, equal the energy, $h\nu$, of the ionizing X-ray quantum.

instead of the intensity variation of the transmitted X-radiation or the voltage required for excitation of an X-ray line. The principles of the present method have been described previously (4, 5, 6). In Fig. 1 is shown a schematic drawing of the experimental set-up. Characteristic radiation from the target of an X-ray tube ejects photo electrons from a converter. The kinetic energy, E_{photo}, of the photo electrons is determined with an iron-free, double focussing β-spectrometer. As illustrated in Fig. 2 the binding energy, B.E., relative to the Fermi level, is obtained by subtracting from the energy, $h\nu$, of the ionizing X-radiation not only E_{photo}, but also the work function of the spectrometer material:

$$\text{B.E.} = h\nu - E_{photo} - \phi_{sp}. \tag{1}$$

It is true that the kinetic energy of a photo electron initially depends upon the work function of the sample, but during the major part of the energy analysis the electron is sensing the vacuum potential of the *spectrometer*.

II. Experimental conditions

A. *Analysis of the electron lines*

The shape of a photo electron line is determined by the shape of the X-ray line used for the production of photo electrons, the energy distribution within the ionized level, the spectrometer window curve, and finally by the energy distribution of electrons scattered inelastically in the source.

For elements with atomic numbers higher than ≈ 30, the profile of the $K\alpha_1$ line follows a Laurentz distribution

$$y = \frac{1}{1+x^2}.$$

This has also been shown theoretically by Weisskopf and Wigner (7) on basic quantum mechanical reasoning. For lower atomic numbers the $K\alpha_1$ X-ray lines exhibit a

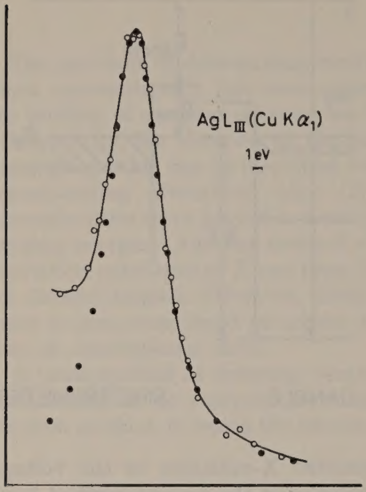

Fig. 3. AgL_{III}(Cu$K\alpha_1$) photo line (open circles) obtained experimentally and a Lorentzian (filled circles) fitted to the high energy flank of the photo line. The deviations of the experimental curve from the symmetrical distribution are explained by the presence of inelastically scattered electrons.

certain asymmetry, which is greatest for the element iron. The index of asymmetry has been defined as the ratio of that part of the full width at half maximum lying on the low energy side of the maximum ordinate to that on the high energy side. This index is as low as 1.12 for the Cu$K\alpha_1$ line (8). Hence, the asymmetry of this line is so small that the Laurentz distribution is still a good approximation of the profile. This can also be assumed to be the case for the energy distribution of the ionized shell. Since a fold of two Laurentz functions gives the same type of function (the width of which is the sum of the partial widths), the "natural" shape of a photo electron line is well-approximated by a Laurentz distribution. An underlying assumption is that the energy level to which the measurements are referred, viz., the vacuum level of the spectrometer, is sharp.

A photo line due to electrons expelled from the L_{III} shell of silver by copper $K\alpha_1$ radiation is shown in Fig. 3. The open circles represent observed points, while the filled circles denote calculated points, obtained by fitting a Laurentzian to the high energy flank of the photo line. The deviations of the experimental curve from the symmetrical distribution on the low energy side are well explained by the presence of electrons that have suffered characteristic energy losses (see below). Hence, it seems quite safe to assume that the spectrometer window curve has a symmetric profile which does not differ greatly from that of a Laurentzian. (Cf. also ref. (6).) It might be added that about 50 per cent of the line width is caused by spectrometer broadening, while the remaining 50 per cent originate from the widths of the Cu$K\alpha_1$ line and the AgL_{III} level.

Characteristic energy losses

According to the preceding discussion, the main cause of the observed asymmetries of the electron lines are the satellites from inelastically scattered electrons. Much attention has been paid during the last ten years to the energy losses suffered by electrons of nonrelativistic energies passing through matter. This may true partly because a thorough understanding of the elementary processes involved is essential for the future development of electron microscopy. The first extensive study of energy losses of electrons scattered from the surface of a solid was made as early as 1929 by Rudberg. An excellent review of the experimental work in this field, as well as the theoretical problems involved, is given by Marton et al. in reference (9). Although the details of the experimental findings differ from author to author, some general observations may be summarized.

The general appearance of an energy loss spectrum is a sequence of characteristic energy loss peaks, which are in many cases superimposed upon a continuous background of inelastically scattered electrons. The characteristic energy loss values are found to depend only upon the composition of the scattering material and are independent of the primary energy of the electrons, thickness of scatterer, and angle of observation. There have been attempts to correlate the characteristic energy losses to soft X-ray levels and interband transitions, and to explain the losses on a collective model as caused by excitations of the electron plasma, a phenomenon that would be analogous to the Čerenkov effect (10). A number of authors (12, 11, 9) have compared the observed energy losses to the free electron plasma frequency

$$\omega = \left(\frac{4\pi n e^2}{m}\right)^{\frac{1}{2}}. \tag{2}$$

Here n is the mean density of free electrons, and e and m the electronic charge and mass. The agreement between the experimental values and those calculated from equation (2) is found to be reasonably good for many elements, but in a number of cases the agreement is poor. However, in the application of equation (2) it has been assumed that n is given by the number of valence electrons; moreover, an underlying assumption is that no coupling exists between the electron plasma and the core electrons; hence this simplified model can be foreseen to fail in many cases.

Experimentally, the half widths of the energy loss peaks are usually broader than the elastic peak width. This is expected if there is an interaction between the plasma and the rest of the solid. It may also be noted that for most elements the main energy loss is about 20 eV.

The total intensity of the inelastically scattered electrons decreases with increasing primary energy and increases with thickness of the specimen. The minimum thickness for energy losses to be observed is considerably less than 100 Å for electrons having energies below 10 keV. The thickness effect for specimens used in the present type of investigation is demonstrated in Fig. 4. For both types of converters the number of electrons that have suffered energy losses less than ≈ 20 eV is small, while the intensity of electrons that have suffered greater energy losses is considerably higher for the thick converter. We must now consider to what extent the photo line peaks are shifted because of the presence of inelastically scattered electrons. If we assume that the first characteristic energy loss line has a Laurentz distribution (displaced a distance x_0 from the elastic peak, peak height equal to I, and half width ω—all quantities relative to those of the elastic line), then the total profile, disregarding the subsequent characteristic energy losses as well as the inelastic background scattering, is obtained as the sum

$$y = \frac{1}{1+x^2} + \frac{I}{1+\left(\frac{x+x_0}{\omega}\right)^2}. \tag{3}$$

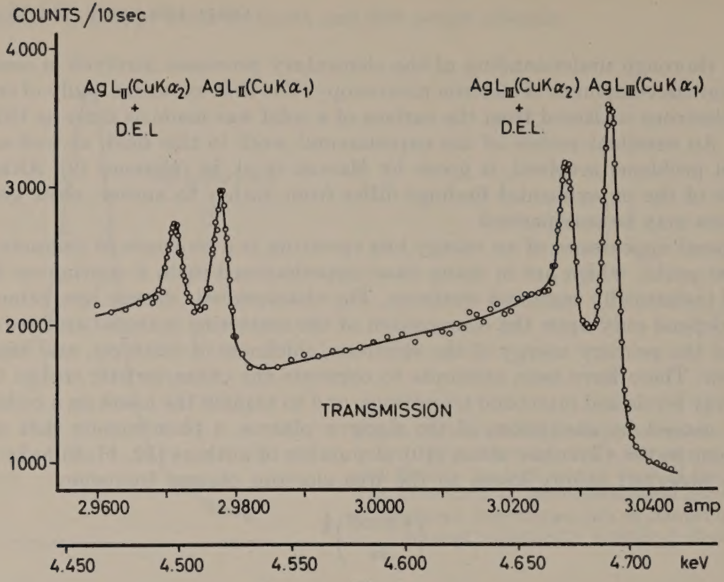

Fig. 4*a*.

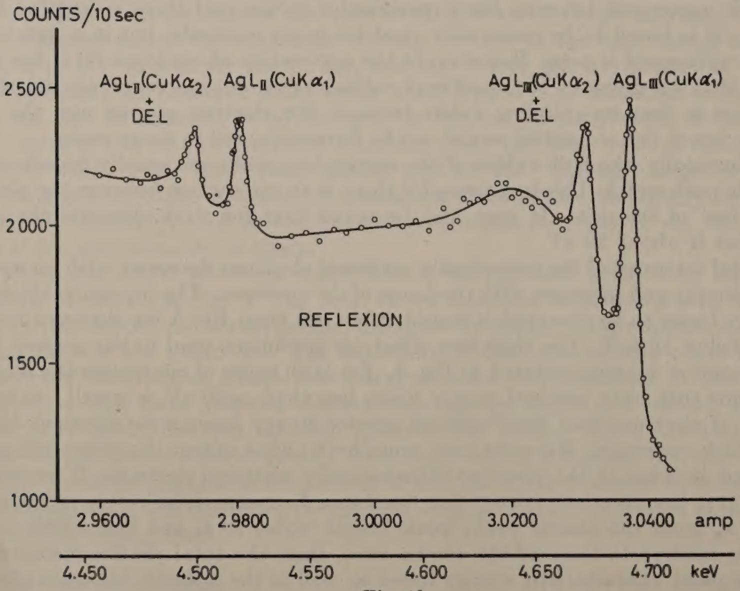

Fig. 4*b*.

Fig. 4. Photo electron lines from the L_{II} and L_{III} shells of silver. Copper $K\alpha$ radiation was used for the production of photo electrons. The curve shown in Fig. 4*a* was obtained from a thin layer of silver, evaporated onto a 15 μ aluminum backing; the spectrum in Fig. 4*b* was obtained from an infinitely thick silver converter. The intensity of inelastically scattered electrons is much higher for the thick converter, but the "elastic" peaks are not seriously disturbed, since no electrons suffer energy losses less than approximately 20 eV.

Derivation of this function with respect to the energy, x, gives for the shift Δx of the elastic line maximum

$$\Delta x = -\frac{I x_0 \omega^2}{(x_0^2+\omega^2)^2 + I\omega^2} \approx -\frac{I x_0 \omega^2}{(x_0^2+\omega^2)^2} \tag{4}$$

if $\Delta x < 1$. This shift is negligibly small for the majority of photo lines obtained in the present investigation. Moreover, there are always *two* lines involved in the energy determination, both subject to the same type of shift. In many cases this will reduce the error completely if the energy determination is made with a calibration line. The most disadvantageous situation is that of the $\mathrm{Te}L_{\mathrm{III}}(\mathrm{Cu}K\alpha_1,\ \mathrm{Mo}K\alpha_1)$ absolute calibration shown in Fig. 8, section (IV A). Here the $\mathrm{Te}L_{\mathrm{III}}(\mathrm{Cu}K\alpha_1)$ photo line is well-resolved from the first characteristic energy loss peak, whereas the $\mathrm{Te}L_{\mathrm{III}}$ $(\mathrm{Mo}K\alpha_1)$ line is disturbed by inelastically scattered electrons to a higher extent than any other photo line obtained in this investigation. If, for this line, the first characteristic loss peak is equally high ($I = 1$) and twice as broad ($\omega = 2$) as the undisturbed line, then equation (4) gives

$$\Delta x = -0.12$$

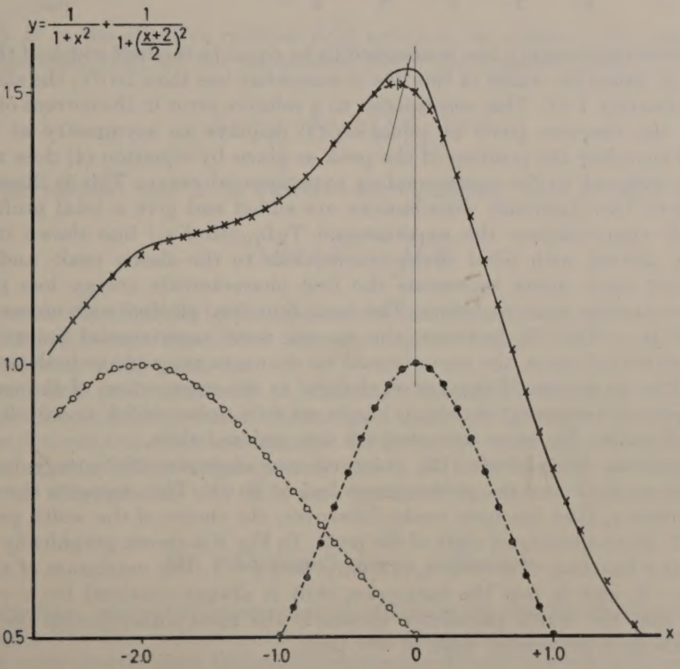

Fig. 5. Addition of two Lorentz distributions. The curve plotted with filled circles corresponds to the undisturbed electron line, and that plotted with open circles to the first characteristic energy loss. The peak of the total profile (crosses) is shifted 6 per cent of the half width of the undisturbed line. Because of the asymmetry at the very peak, the shift of the corresponding experimental curve (full line) is smaller.

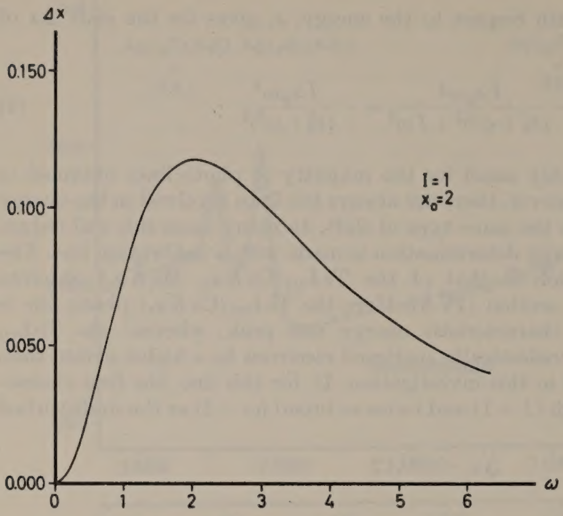

Fig. 6. Peak shift of total profile curve as a function of the half width of the characteristic loss line.

if the characteristic energy loss is assumed to be equal to the half width of the elastic line ($x_0 = 2$). Since the width of this line is somewhat less than 20 eV, the shift would be approximately 1 eV. This corresponds to a relative error in the current of 4×10^{-5}. However, the function given by equation (3) displays an asymmetry at the very peak, and therefore the position of the peak as given by equation (4) does not agree with that assigned to the corresponding experimental curve. This is illustrated in Fig. 5. Here two Laurentz distributions are added and give a total profile which fairly well approximates the experimental $\mathrm{Te}L_{\mathrm{III}}(\mathrm{Mo}K\alpha_1)$ line shown in Fig. 8. The curve plotted with filled circles corresponds to the elastic peak, and the one plotted with open circles represents the first characteristic energy loss peak; the parameters are the same as before. The total function, plotted with crosses, has its maximum at -0.12. If, however, the crosses were experimental points with an inherent statistical error, the curve should be drawn in principle as indicated by the full line. The maximum of this curve, defined as the intersection of the curve with the diameter of horizontal chords, is displaced 0.06 units, which is only 3 per cent of the half width. We have corrected for this residual shift.

For tellurium, Möllenstedt (13) observed two characteristic energy losses, one very weak at 8 eV and the predominant loss at 20 eV. This supports the choice of the parameter x_0 that has been made. Moreover, the choice of the width parameter, $\omega = x_0 = 2$, gives the largest shift of the peak. In Fig. 6 is shown graphically the peak shift Δx as a function of ω with $x_0 = 2$ units and $I = 1$. The maximum of this curve falls at $\omega = 2$, and in fact the maximum shift is always obtained for $\omega = x_0$. This indicates that the width parameter chosen is the most unfavourable one since it corresponds to a maximum shift of the peak.

B. *Residual Magnetic Field*

Prior to turning on the spectrometer field, one must compensate for all external magnetic field components, including the earth magnetic field as well as stray fields from magnets in other laboratories. As described in reference (4), this is achieved with three pairs of Helmholtz coils. When all external magnetic fields are balanced out at the center of the spectrometer, a small residual field along the electron trajectory still remains. The axial component of this field was found (14) to vary periodically with a maximum value of 3.5×10^{-3} gauss. In order to obtain the *constant* field B', which would have the same effect as the actual residual field, this must be weighted with a certain function. The appropriate weighting function can be calculated (15) or may be determined experimentally. Sokolowski (6), experimentally found a weighting function that yielded a value for the *effective* residual field

$$B' = 7.0 \times 10^{-4} \text{ gauss.}$$

If the current for which electrons of momentum $B\varrho$ are focussed in the spectrometer is denoted by I, and $\varkappa$ is the calibration constant of the spectrometer ($\varkappa$ is a constant only for a given position of source and detector), the $B\varrho$ values for the calibration line and the line to be examined are given by

$$\left.\begin{aligned} B\varrho_c &= \varkappa I_c + \varrho B' \\ B\varrho &= \varkappa I + \varrho B' \end{aligned}\right\} \tag{5}$$

in which B' is the effective residual field and ϱ is the radius of the spectrometer. These equations yield for the momentum $B\varrho$ of the examined line

$$B\varrho = \frac{I}{I_c} \cdot B\varrho_c + \left(1 - \frac{I}{I_c}\right) \varrho B'. \tag{6}$$

Hence, the residual field B' is corrected for by adding (with its sign) a quantity

$$\Delta B\varrho = \left(1 - \frac{I}{I_c}\right) \varrho B' \tag{7}$$

to the momentum obtained by multiplying the current ratio I/I_c with the momentum $B\varrho_c$ of the calibration line. Since the spectrometer radius is 30 cm, the quantity $\varrho B'$ amounts to 0.021 gauss-cm.

It would first seem preferable to adjust the magnetic field at the center of the spectrometer to a nonzero value which would make corrections for the residual field along the electron trajectory superfluous. However, the instrument used for balancing out the magnetic field, a magnetometer type 1.100 from Institut Dr Förster, Reutlingen, was fully reliable only as a zero indicator, because of aging effects in the probe.

III. "Absolute" energy calibration

An "absolute" method of determining $B\varrho$ values of electron lines has been described by Siegbahn (16). This method is absolute in the sense that no separate determinations of B and ϱ are needed, since the measurements are directly related to X-ray energies, often known with an accuracy of one or two parts in 10^5. In β-spectroscopic work this method is applied by recording conversion lines from two different shells of the same γ-transition, and then calculating the energies of the electron lines, by use of the known energy of the corresponding X-ray transition. This transition might be forbidden by selection rules, but often, especially for heavy elements, can be obtained by proper combinations of allowed transitions. When an iron-free spectrometer is used, only the ratio of the currents of the electron line peaks enters the calculations. In this way several conversion lines in the Th B+C spectrum have been determined by Siegbahn and Edvarson (14). They also discuss the errors pertaining to the measurements. The formulae which they give for the error calculation are valid even for relativistic energies.

Two absolute energy determinations with the Siegbahn method have been performed in the present investigation. Here, a slightly different approach has been used. Instead of having electromagnetic radiation of a certain wavelength converted in *two different* shells of an element, the anode of the X-ray tube consisted of two different elements, and the photo electron lines due to conversion of the $K\alpha_1$-radiation from both target materials in *the same* shell of the converter atoms were recorded. The K and L_{III} energies of copper and tellurium respectively were determined (section IV, A).

A. *Error calculation*

For the energies involved in the present investigation an unrelativistic error calculation was found to be valid.

If ν is the frequency difference between the two X-ray lines that are used for the production of photo electrons and α the ratio I_2/I_1 of the currents pertaining to the photo line peaks, recorded with the iron-free spectrometer, then the $B\varrho$ value of the low energy line is given unrelativistically by the expression

$$B\varrho_1^2 = 2 \cdot \frac{h}{e} \cdot \frac{m}{e} \cdot \nu \cdot \frac{1}{\alpha^2 - 1} \tag{8}$$

The relative error of the momentum becomes

$$\frac{\Delta B\varrho_1}{B\varrho_1} = 0.5\,\frac{\Delta h/e}{h/e} + 0.5\,\frac{\Delta m/e}{m/e} + 0.5\,\frac{\Delta \nu}{\nu} - \frac{\alpha^2}{\alpha^2 - 1}\,\frac{\Delta\alpha}{\alpha}. \tag{9}$$

In contrast to the corresponding relativistic formula the coefficients of the three first terms in equation (9) are all constant and equal to 0.5. The relativistic expression for the coefficient of $\Delta\alpha/\alpha$ is obtained by multiplying the unrelativistic quantity $-\alpha^2/(\alpha^2-1)$ by a factor

$$R = \frac{3 + \alpha^2 + \dfrac{1.17 \cdot 10^7}{B\varrho^2}}{\sqrt{(\alpha^2+1)^2 + \dfrac{1.05\,(\alpha^2-1)^2}{\Delta^2}}} \tag{10}$$

Here $B\varrho$ is the momentum of the low energy line expressed in gauss-cm, and Δ is the energy difference between the two photo lines expressed in eV.

A check to determine how high in energy error calculations can be made with equation (9) is given by a comparison of the expressions obtained with this equation to those of the relativistic formula in reference (14). For the I and F lines of ThB, the following expression is given in reference (14):

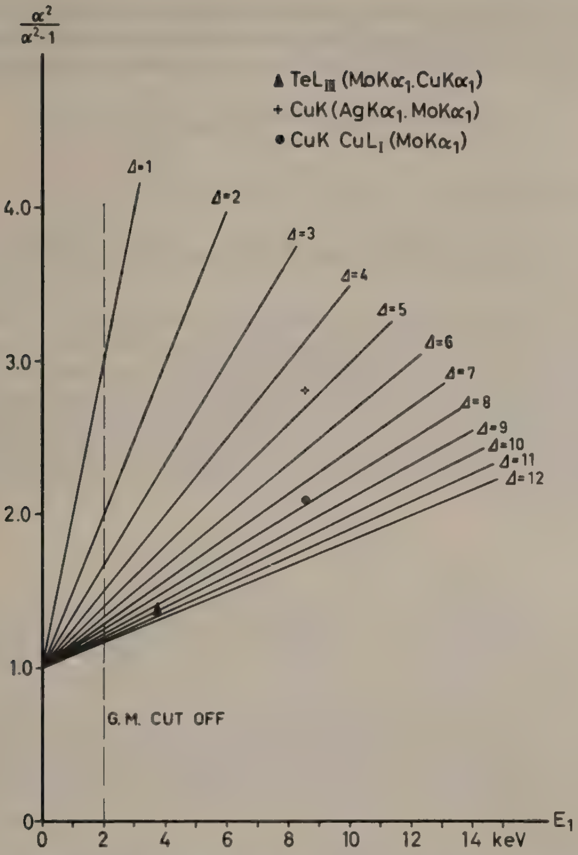

Fig. 7. Relative accuracy of "absolute" $B\varrho$-determinations in the unrelativistic range. The relative error in the moment um of thelow energy line is proportional to the quantity $\alpha^2/(\alpha^2-1)$. This factor is shown in the figure as a function of the energy E_1 of the low energy line for various energy differences, Δ, between the photo lines.

$$\frac{\Delta B\varrho}{B\varrho} = 0.65\,\frac{\Delta h/e}{h/e} + 0.35\,\frac{\Delta m/e}{m/e} + 0.65\,\frac{\Delta \nu}{\nu} - 3.3\,\frac{\Delta \alpha}{\alpha} \tag{11}$$

as compared to

$$\frac{\Delta B\varrho}{B\varrho} = 0.50\,\frac{\Delta h/e}{h/e} + 0.50\,\frac{\Delta m/e}{m/e} + 0.50\,\frac{\Delta \nu}{\nu} - 2.7\,\frac{\Delta \alpha}{\alpha} \tag{12}$$

obtained from equation (9). In this case, in which the energies are of the order of 100 keV, it is evident that the relativistic formula must be used.

Another absolute energy determination is discussed in reference (4). This is concerned with CuK- and CuL_1 photo electrons expelled by Mo$K\alpha_1$ radiation. Here the electron energies are 8.5 and 16.4 keV, and the relativistic formula gives

$$\frac{\Delta B\varrho}{B\varrho}=0.52\,\frac{\Delta h/e}{h/e}+0.47\,\frac{\Delta m/e}{m/e}+0.52\,\frac{\Delta\nu}{\nu}-2.1\,\frac{\Delta\alpha}{\alpha} \tag{13}$$

whereas equation (9) gives

$$\frac{\Delta B\varrho}{B\varrho}=0.50\,\frac{\Delta h/e}{h/e}+0.50\,\frac{\Delta m/e}{m/e}+0.50\,\frac{\Delta\nu}{\nu}-2.1\,\frac{\Delta\alpha}{\alpha} \tag{14}$$

The coefficients of the three first terms differ by only ≈ 5 per cent, and the coefficient for $\Delta\alpha/\alpha$ becomes the same value in both cases. The energies involved in the two absolute calibrations made in the present investigation are lower than those of the Cu$K$Cu$L_{\rm I}$(Mo$K\alpha_1$) calibration, and hence equation (9) is valid to a high degree of precision, especially for the last term. Uncertainties in the elementary constants and X-ray data will subsequently be neglected in the error calculation.

The coefficient of the last term in equation (9) is shown graphically in Fig. 7. This can be written as

$$\frac{\alpha^2}{\alpha^2-1}=1+\frac{E_1}{\Delta} \tag{15}$$

in which E_1 corresponds to the low energy line, and Δ is the energy difference between the photo electron lines. The proper values for the absolute calibrations made in this investigation as well as that of the Cu$K$Cu$L_{\rm I}$(Mo$K\alpha_1$) calibration mentioned earlier are marked. When $\Delta\alpha/\alpha$ is assumed to be the same in all three cases, the Te$L_{\rm III}$(Cu$K\alpha_1$Mo$K\alpha_1$) calibration gives the smallest relative error, 1.4 $\Delta\alpha/\alpha$. Since the energy E_1 of the Te$L_{\rm III}$(Cu$K\alpha_1$) line is about 3.7 keV as compared to 8.5 keV for the CuK(Mo$K\alpha_1$) line, the absolute error in energy for the Te$L_{\rm III}$ (Cu$K\alpha_1$Mo$K\alpha_1$) calibration is only one-fifth of that of the CuK(Mo$K\alpha_1$Ag$K\alpha_1$) calibration.

B. *Residual field correction*

For the energies included in Fig. 7, the error made by using the unrelativistic expression is less than 5 percent ($|R-1|<0.05$). This makes possible the use of equation (9) not only for error calculation, but also for corrections, e.g., for the residual magnetic field.

Equations (5) are rewritten as

$$\left.\begin{aligned}B\varrho_1&=\varkappa I_1+\varrho B'\\ B\varrho_2&=\varkappa I_2+\varrho B'\end{aligned}\right\} \tag{16}$$

in which indices 1 and 2 are related to the low and high energy lines, respectively. These equations are solved for $\Delta\alpha/\alpha=(I_2/I_1-B\varrho_2/B\varrho_1)/I_2/I_1$ with the assumption that $(\varrho B')^2\ll(B\varrho_1)^2$:

$$\frac{\Delta\alpha}{\alpha}=\frac{\alpha-1}{\alpha}\cdot\frac{\varrho B'}{B\varrho_1}. \tag{17}$$

Thus, the error arising from the residual magnetic field is interpreted as an error in the current ratio, α. Then equations (9) and (17) give corrections which must be added to the momenta of the two photo lines:

$$\begin{aligned} \Delta B\varrho_1 &= \frac{\alpha}{\alpha+1}\cdot \varrho B' \\ \Delta B\varrho_2 &= \frac{1}{\alpha+1}\cdot \varrho B' \end{aligned} \tag{18}$$

Hence, the corrections are always smaller than $\varrho B' = 0.021$ gauss-cm.

IV. Experimental results

A. *The calibration lines*

Table 1 lists the wavelengths and energies of the X-ray lines that have been used for the production of photo electrons. The wavelength values are those given by Sandström in reference (2). Recently Beckman *et al.* (17) have remeasured the silver line. They suggest a somewhat lower wavelength value than that in Table 1. However, the difference is only about one part in 10^5. DuMond and Cohen's list of atomic constants, published in 1953 (18), has been used for all calculations in the present investigation. One reason for this is that the conversion from momentum to energy has been carried out with the aid of the tables in reference (19), and these tables were calculated with the 1953 list. The accuracy of the tables is very high and allows for an interpolation to the second order. This was found to be necessary in many cases; the electron energy, E, corresponding to a given $B\varrho$ value then is obtained from the formula

Table 1.

X-ray line	Wavelength (x.u.)	Energy (eV)
$\mathrm{Cu}\,K\alpha_1$	1537.396	8047.5
$\mathrm{Mo}\,\mathrm{K}\alpha_1$	707.831	17479.0
$\mathrm{Ag}\,\mathrm{K}\alpha_1$	558.253	22162.4

$$E = E_0 + xF_0 + \frac{x^2}{2h}(F_0 - F_{-1}), \tag{19}$$

in which x is the difference $B\varrho - B\varrho_0$, and h is $B\varrho_0 - B\varrho_{-1}$; E_n and F_n are tabulated as functions of $B\varrho_n$.

1. $\mathrm{Te}\,L_{\mathrm{III}}(\mathrm{Cu}\,K\alpha_1,\ \mathrm{Mo}\,K\alpha_1)$

For the $\mathrm{Te}\,L_{\mathrm{III}}(\mathrm{Cu}\,K\alpha_1\,\mathrm{Mo}\,K\alpha_1)$ calibration an anode was made of copper with molybdenum slabs pressed into grooves in the copper. The $\mathrm{Te}\,L_{\mathrm{III}}(\mathrm{Cu}\,K\alpha_1)$ and $\mathrm{Te}\,L_{\mathrm{III}}(\mathrm{Mo}\,K\alpha_1)$ lines were recorded (Fig. 8) and their $B\varrho$ values determined, by use of the known energies of the $\mathrm{Cu}\,K\alpha_1$ and $\mathrm{Mo}\,K\alpha_1$ radiation. It should be pointed

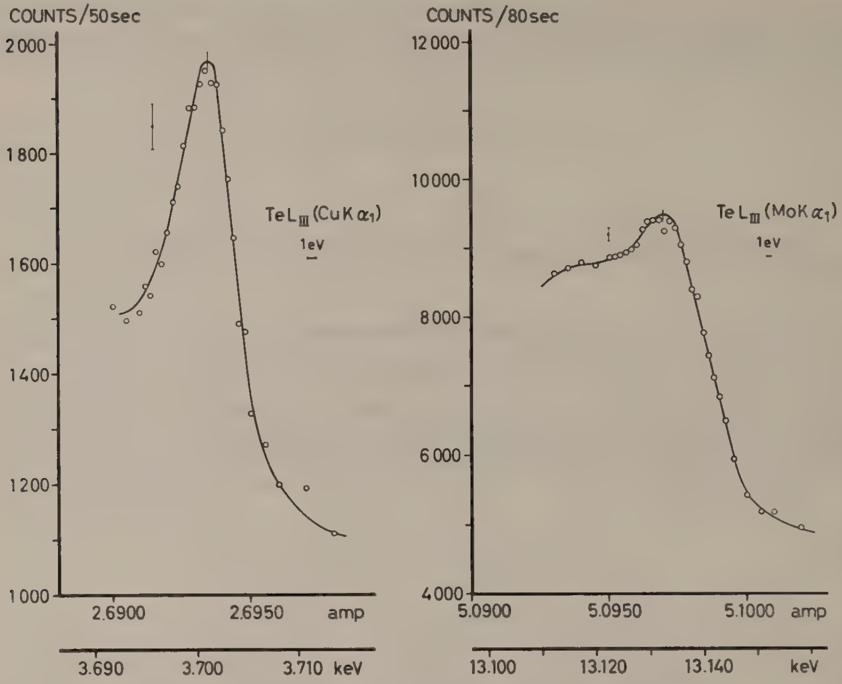

Fig. 8. Photo lines of the TeL_{III}(Cu$K\alpha_1$, Mo$K\alpha_1$) calibration.

out that it is preferable to carry out the evaluation of the $B\varrho$ values with successive approximations rather than by calculations from relativistic formulae. In fact, the calibration constant is always so well-known that the proper $B\varrho$ values can be obtained in the second step, if the relative error in momentum is considered one-half of the relative error in the energy difference (equation (9)).

Two measurements were made of the TeL_{III}(Cu$K\alpha_1$ Mo$K\alpha_1$) lines; the relevant data are given in Table 2. Correction for the effective residual magnetic field has been

Table 2.

$I_{\mathrm{Te}L_{III}(\mathrm{Cu}K\alpha_1)}$ (amps)	$I_{\mathrm{Te}L_{III}(\mathrm{Mo}K\alpha_1)}$ (amps)	$B\varrho_{\mathrm{Te}L_{III}(\mathrm{Cu}K\alpha_1)}$ (gauss-cm)
2.69350	5.09698	205.517
2.69558	5.10080	205.524
	Mean value	205.520
Mean value corrected for residual magnetic field		205.534 ± 0.012

applied according to equation (18). Only those errors pertaining to the present measurements are considered, while the uncertainties in the elementary constants and X-ray emission lines are disregarded. The error in the current attributed to the peak of an electron line is here set to be one-twentieth of the half width (confer section IV B1); the relative error $\Delta\alpha/\alpha$ of the current ratio then is obtained by quadratic addition. This $\Delta\alpha/\alpha$-value is inserted into equation (9) and gives

$$\Delta B\varrho_1 = \pm B\varrho_1 \cdot \frac{\alpha^2}{\alpha^2-1}\,\frac{\Delta\alpha}{\alpha}. \tag{20}$$

Finally, the error assigned to the mean value of the two measurements is obtained by division with $\sqrt{2}$. The relative error in momentum of the TeL_{III}(Cu $K\alpha_1$) line, calculated in this way, is as small as 5×10^{-5}, which corresponds to an error in energy of only four-tenths of an electron volt.

Using the $B\varrho$ value 205.534 gauss-cm of the TeL_{III}(Cu $K\alpha_1$) line, we can calculate the momentum of the A6 line in the Auger spectrum of copper (4), since these two electron lines have been measured relative to each other. From Table 21 in section (IV B 3) we obtain a mean current ratio $I_{\text{A6}}/I_{\text{Te}} = 1.38083 \pm 0.00003$, and after we correct for the residual magnetic field according to equation (7), we get

$$B\varrho_{\text{A6}} = 283.800 \pm 0.017 \text{ gauss-cm.}$$

Table 3.

$I_{\text{Cu}\,K\,(\text{Mo}\,K\alpha_1)}$ (amps)	$I_{\text{Cu A6}}$ (amps)	α
4.08975	3.71890	1.099720
4.08970	3.71890	1.099707
4.08855	3.71800	1.099664
4.08840	3.71763	1.099733
Mean value		1.099706 ± 0.000030

Finally, a $B\varrho$ value for the Cu K(Mo $K\alpha_1$) line is obtained from the data given in Table 3. Here four measurements of the CuA6 Auger line with respect to the Cu K (Mo $K\alpha_1$) line are listed. These are taken from data underlying the energy shift determinations in reference (5); the photo- and Auger lines in those cases were determined in the same measurement. From the mean current ratio $\bar{\alpha} = 1.099706$ in Table 3 and the $B\varrho$ value 283.800 gauss-cm of the CuA6 line, the value for the Cu K (Mo $K\alpha_1$) line after correction for residual field becomes:

$$B\varrho_{\text{Cu}\,K\,(\text{Mo}\,K\alpha_1)} = 312.095 \pm 0.020 \text{ gauss-cm.}$$

2. Cu K (Mo $K\alpha_1$, Ag $K\alpha_1$)

Since a number of electron lines were measured relative to the Cu K (Mo $K\alpha_1$) line, an absolute determination of this line was also performed with the use of a molybdenum–silver anode. One of the measurements is illustrated in Fig. 9. Five measurements listed in Table 4, were made. As seen in Fig. 7, the accuracy of this calibration

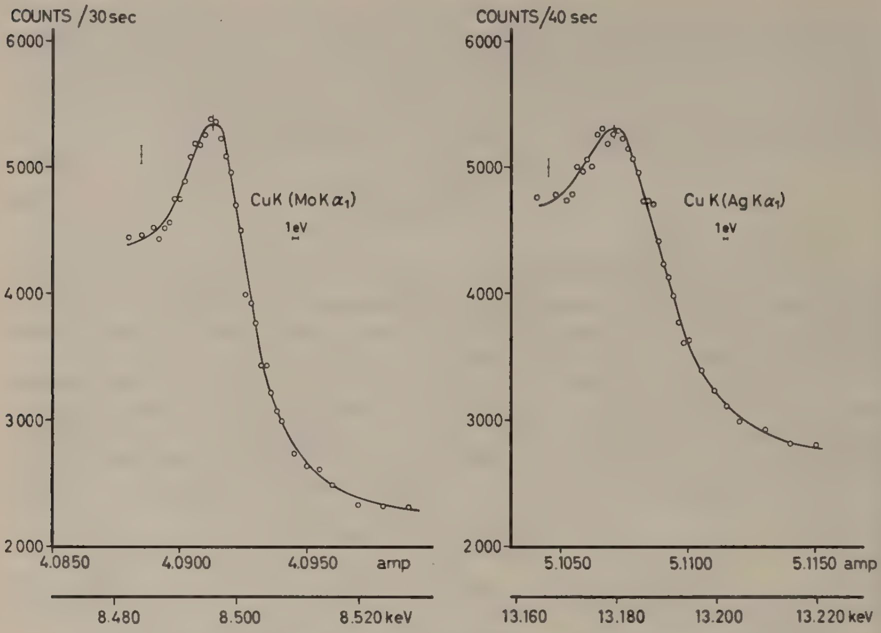

Fig. 9. Photo lines of the Cu K (Mo $K\alpha_1$ Ag $K\alpha_1$) calibration.

is rather low; and although five calibrations were carried out, the relative error is larger than that of the TeL_{III}(Cu $K\alpha_1$ Mo $K\alpha_1$) calibration.

Sokolowski (6) has applied the residual field correction to the momentum given in reference (4) for the Cu K (Mo $K\alpha_1$) line. This yields a value 312.086 ± 0.017 gauss-cm. Two additional momentum values of the CuA6 line can now be obtained from the $B\varrho$ value 312.117 gauss-cm of the Cu K(Mo $K\alpha_1$ Ag $K\alpha_1$) calibration and the value

Table 4.

$I_{\mathrm{Cu}\,K\,(\mathrm{Mo}\,K\alpha_1)}$ (amps)	$I_{\mathrm{Cu}\,K\,(\mathrm{Ag}\,K\alpha_1)}$ (amps)	$B\varrho_{\mathrm{Cu}\,K\,(\mathrm{Mo}\,K\alpha_1)}$ (gauss-cm)
4.09230	5.10850	312.103
4.09000	5.10552	312.121
4.09048	5.10632	312.087
4.09190	5.10812	312.082
4.09130	5.10708	312.130
	Mean value	312.105
Mean value corrected for residual magnetic field		312.117 ± 0.022

Table 5.

Line	Process of determination	$B\varrho$ (gauss-cm)	Weighted mean (gauss-cm)
Cu A6	Rel. Te L_{III} (Cu $K\alpha_1$) determined abs. from Te L_{III} (Cu $K\alpha_1$ Mo $K\alpha_1$)	283.800 ± 0.017	283.803 ± 0.010
	Rel. Cu K (Mo $K\alpha_1$) determined abs. from Cu K (Mo $K\alpha_1$ Ag $K\alpha_1$)	283.821 ± 0.020	
	Rel. Cu K (Mo $K\alpha_1$) calibrated against F line in ThB	283.792 ± 0.017	
Cu K (Mo $K\alpha_1$)	Abs. from Cu K (Mo $K\alpha_1$ Ag $K\alpha_1$)	312.117 ± 0.022	312.097 ± 0.012
	Rel. F line in ThB	312.086 ± 0.017	
	Via Cu A6 rel. Te L_{III} (Cu $K\alpha_1$) determined abs. from Te L_{III} (Cu $K\alpha_1$ Mo $K\alpha_1$).	312.095 ± 0.020	

312.086 gauss-cm of the calibration against the F line in ThB. After dividing these numbers by $\alpha = 1.099706$ and correcting for residual field, we then get:

$$B\varrho_{A6} = 283.821 \pm 0.020 \text{ gauss-cm}$$

$$\text{and} \quad B\varrho_{A6} = 283.792 \pm 0.017 \text{ gauss-cm}$$

respectively. The $B\varrho$ values of the reference lines, resulting from the different processes of determination, are listed in Table 5. All values agree to within experimental errors. It should also be emphasized that errors in elementary constants and X-ray data are not taken into account.

B. *Binding energies*

The energy determinations were carried out in essentially the same way as described in reference (5), by use of a triple source holder with evaporated layers of the calibration substance and the element to be investigated. In most cases the CuA6 line was used as a reference. It is advantageous to take calibration lines from Auger spectra, since the energy of an Auger line is independent of the wavelength of the ionizing X-radiation. This simplifies the choice of target material for the X-ray tube.

For each element the binding energy determinations were made with at least two samples. The number of the sample used in each case is given in the second column of the tables. In the following columns are listed: (i) current of photo line, (ii) current of calibration line, (iii) $B\varrho$ value of photo line, corrected for residual field, and (iv) corresponding energy of photo line.

1. *Error estimation*

For the fifth period elements practically all $B\varrho$ values listed deviate from the mean value less than 4 parts in 10^5. This corresponds to a maximum uncertainty in the localization of a photo or Auger line peak of approximately 1/30 of the half width (defined as twice the width of the high energy flank). Since four measurements are made for each energy (except for the SnL_{I}, SnL_{II} and AgL_{II} energies), the relative error assigned to the mean value of the photo electron momentum is 2×10^{-5}. In the elements of the fourth period the reproducibility is somewhat lower because of the greater half width of the photo lines. Here the relative error in the mean of four measurements is set to be 3×10^{-5}. Hence, the relative errors in *energy* are 4×10^{-5} and 6×10^{-5}, respectively. It should be kept in mind that these relative errors pertain to the energies of the *photo lines*. The quantity (B.E. $+ \phi_{\mathrm{sp}}$), given below each table, is obtained by subtracting the mean value of the photo line energy from the pertinent X-ray energy. Here the errors include not only those deduced from the reproducibility, but also the errors given in Table 5 for the calibration lines. The current control is performed with an AEG compensator as described in reference (14). A test of the consistency of the decades indicated that the relative error in the current ratio α due to uncertainties in the relative values of the resistors was always less than 2×10^{-5}. These errors have not been included.

2. *Fourth period elements*

30. Zn

Table 6. Zn K (Mo $K\alpha_1$).

Calibration line	#	$I_{\mathrm{Zn}\,K}$ (amps)	I_c (amps)	$B\varrho$ (gauss-cm)	E_{photo} (eV)
Cu A6	127	3.92155	3.71917	299.245	7815.5
	127	3.92127	3.71915	299.260	7816.2
	128	3.92280	3.72025	299.254	7815.9
Cu K (Mo $K\alpha_1$)	30	3.92050	4.08895	299.241	7815.3
			Mean	299.250 ± 0.009	7815.7 ± 0.5

Zn K: B.E. $+ \phi_{\mathrm{sp}} = 9663.3 \pm 0.8$ eV.

31. Ga

Table 7. Ga K (Mo $K\alpha_1$).

Calibration line	#	$I_{\mathrm{Ga}\,K}$ (amps)	I_c (amps)	$B\varrho$ (gauss-cm)	E_{photo} (eV)
Cu A6	104	3.73830	3.71912	285.267	7107.2
	104	3.73848	3.71916	285.277	7107.7
	123	3.73863	3.71948	285.264	7107.1
Cu K (Mo $K\alpha_1$)	58	3.73740	4.08903	285.261	7106.9
			Mean	285.267 ± 0.009	7107.2 ± 0.4

Ga K: B.E. $+ \phi_{\mathrm{sp}} = 10371.8 \pm 0.7$ eV.

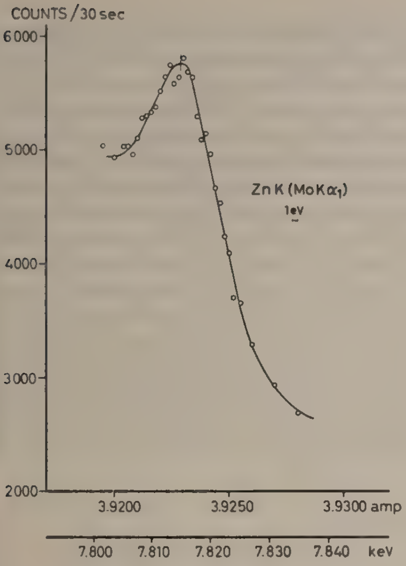

Fig. 10. ZnK(Mo$K\alpha_1$) photo line.

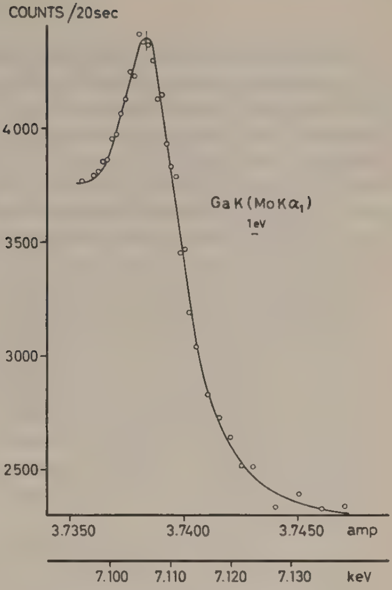

Fig. 11. GaK(Mo$K\alpha_1$) photo line.

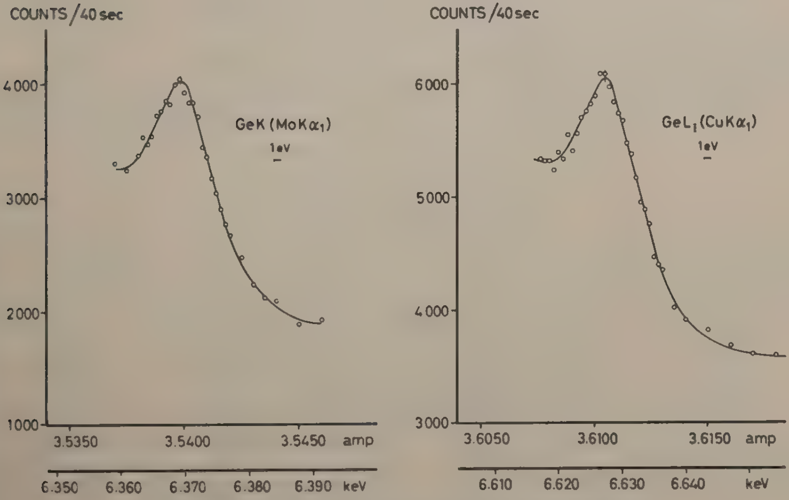

Fig. 12. GeK(Mo$K\alpha_1$)- and GeL_I(Cu$K\alpha_1$) photo lines.

32. Ge

Until the present time there has existed no determination of the L_I binding energy of germanium. As shown in Fig. 12, the GeL_I(Cu$K\alpha_1$) photo line has a high intensity, which renders it suitable for an energy determination. This was performed with the use of the CuA6 and GeA6 Auger lines for the calibration. The $B\varrho$ values of these lines are given in reference (20). The momentum of CuA6 was reconsidered in section (IV A) and yielded a Bϱ value well within the errors given in the earlier publication. The GeA6 line was measured relative to the CuK(Zr$K\alpha_1$) line, while the other Auger lines of the germanium spectrum were measured with GeA6 as a reference. A renewed analysis of the data gives for this line a $B\varrho$ value 313.334 gauss-cm. This value differs slightly from that given in reference (20), since the momentum of the CuK(Mo$K\alpha_1$) line is now set to be 312.097 gauss-cm, and also since another conversion factor from wavelength to energy has been used. Hence, the energies listed in Table 2 of reference (20) should be increased by 1.5 eV. This does not alter the *relative* positions of the lines, and the new energy values always fall well within the errors given in the earlier publication. It is evident from the measurements listed in Tables 8 and 9 that the $B\varrho$ value 313.334 gauss-cm for the GeA6 line yields energy values for the K and L_I electrons in germanium that are consistent with those obtained with other reference lines.

Table 8. GeK(Mo$K\alpha_1$).

Calibration line	#	$I_{\mathrm{Ge}\,K}$ (amps)	I_c (amps)	$B\varrho$ (gauss-cm)	E_{photo} (eV)
CuK(Mo$K\alpha_1$)	31	3.54080	4.09285	270.004	6371.6
	48	3.53983	4.09207	269.981	6370.5
	48	3.53980	4.09213	269.975	6370.3
Ge A6	31	3.54070	4.10930	269.981	6370.5
			Mean	269.985 ± 0.008	6370.7 ± 0.4

GeK: B.E. + ϕ_{sp} = 11108.3 ± 0.6.

Table 9. GeL_I(Cu$K\alpha_1$).

Calibration line	#	$I_{\mathrm{Ge}\,L_I}$ (amps)	I_c (amps)	$B\varrho$ (gauss-cm)	E_{photo} (eV)
Ge A6	36	3.61055	4.10706	275.457	6629.9
	48	3.61138	4.10810	275.451	6629.6
Cu A6	48	3.61138	3.72093	275.448	6629.5
	36	3.61045	3.72028	275.426	6628.4
			Mean	275.446 ± 0.008	6629.3 ± 0.4

Ge L_I: B.E. + ϕ_{sp} = 1418.2 ± 0.7 eV.

34. Se

Three different calibration lines were used for the selenium measurements: namely, the Cu K (Mo $K\alpha_1$), CuA6, and Tl L_{III} (Mo $K\alpha_1$) lines. The third reference line, Tl L_{III} (Mo $K\alpha_1$), was chosen in order to be able to check the consistency with the energy determinations made by Sokolowski in the sixth period (6). The energy difference between this calibration line and Se K (Mo $K\alpha_1$) is as small as about 1 eV. (A slightly different $B\varrho$ value has been assigned to the Tl L_{III} (Mo $K\alpha_1$) line, in accordance with the $B\varrho$ value 312.097 used in the present investigation.) Heating in vacuum af the evaporated samples made sure that they were of the metallic form.

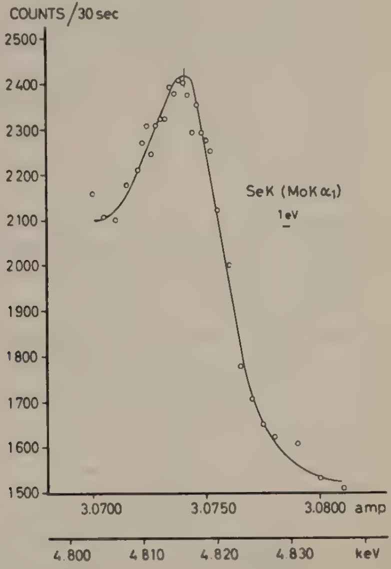

Fig. 13. Se K (Mo $K\alpha_1$) photo line.

Table 10. Se K (Mo $K\alpha_1$).

Calibration line	#	$I_{\mathrm{Se}\,K}$ (amps)	I_c (amps)	$B\varrho$ (gauss-cm)	E_{photo} (eV)
Cu A6	117	3.07485	3.72036	234.565	4816.0
	125	3.07445	3.71935	234.598	4817.4
Cu K (Mo $K\alpha_1$)	65	3.07390	4.08960	234.589	4817.0
Tl L_{III} (Mo $K\alpha_1$)	67	3.07400	3.07465	234.580	4816.7
			Mean	234.583 ± 0.007	4816.8 ± 0.3

Se K: B.E. + $\phi_{sp} = 12662.2 \pm 0.5$ eV.

3. *Fifth period elements*

45. Rh

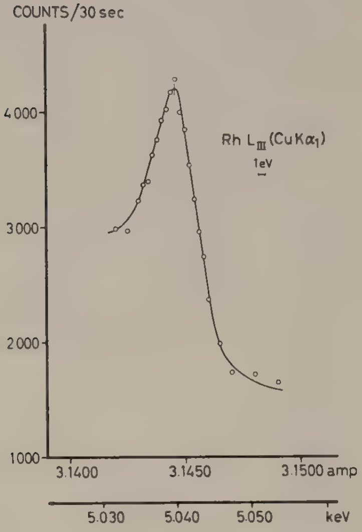

Fig. 14. RhL_{III}(Cu$K\alpha_1$) photo line.

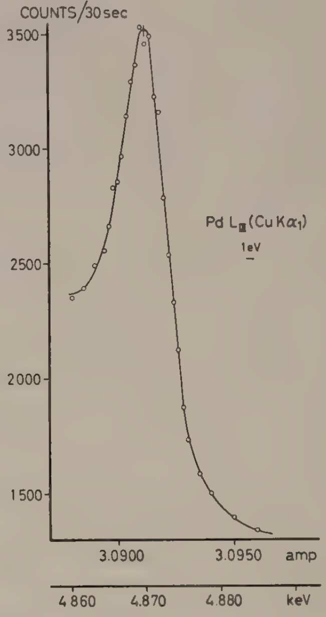

Fig. 15. PdL_{III}(Cu$K\alpha_1$) photo line.

Table 11. Rh L_{III} (Cu $K\alpha_1$).

Calibration line	#	$I_{\mathrm{Rh}\,L_{\mathrm{III}}}$ (amps)	I_c (amps)	$B\varrho$ (gauss-cm)	E_{photo} (eV)
Cu A6	97	3.14432	3.71855	239.980	5039.9
	97	3.14422	3.71857	239.971	5039.5
	99	3.14571	3.72018	239.981	5039.9
	99	3.14572	3.72013	239.985	5040.1
			Mean	239.979 ± 0.005	5039.8 ± 0.2

Rh L_{III}: B.E. + $\phi_{\mathrm{sp}} = 3007.7 \pm 0.5$ eV.

46. Pd

Table 12. Pd L_{III} (Cu $K\alpha_1$).

Calibration line	#	$I_{\mathrm{Pd}L_{III}}$ (amps)	I_c (amps)	$B\varrho$ (gauss-cm)	E_{photo} (eV)
Cu A6	76	3.09123	3.71930	235.882	4870.1
	76	3.09115	3.71928	235.877	4869.9
	95	3.09230	3.72045	235.890	4870.4
	95	3.09232	3.72058	235.884	4870.2
			Mean	235.883 ± 0.005	4870.1 ± 0.2

Pd L_{III}: B.E. $+ \phi_{sp} = 3177.4 \pm 0.5$.

47. Ag

From the data underlying Fig. 4, two determinations of the AgL_{II} energy were made with the AgL_{III} (Cu $K\alpha_1$) line as a reference. The $B\varrho$ value of this line is 231.516 gauss-cm as given in Table 13.

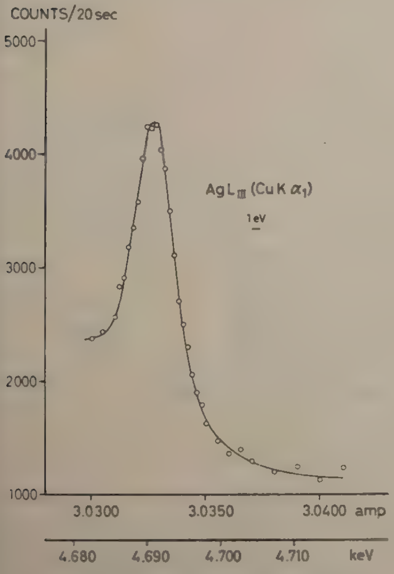

Fig. 16. AgL_{III} (Cu $K\alpha_1$) photo line.

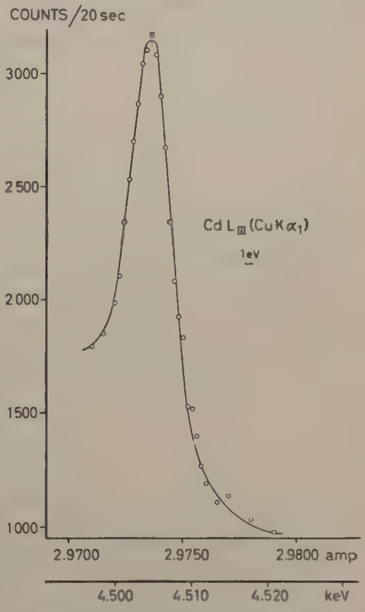

Fig. 17. CdL_{III} (Cu $K\alpha_1$) photo line.

Table 13. Ag L_{III} (Cu $K\alpha_1$).

Calibration line	#	$I_{\mathrm{Ag}\,L_{\mathrm{III}}}$ (amps)	I_c (amps)	$B\varrho$ (gauss-cm)	E_{photo} (eV)
Cu A6	68	3.03276	3.71775	231.517	4692.2
	68	3.03271	3.71780	231.510	4691.9
	80	3.03355	3.71868	231.519	4692.3
	80	3.03534	3.72087	231.519	4692.3
			Mean	231.516 ± 0.005	4692.2 ± 0.2

Ag L_{III}: B.E. + $\phi_{\mathrm{sp}} = 3355.3 \pm 0.5$ eV.

Table 14. Ag L_{II} (Cu $K\alpha_1$).

Calibration line	#	$I_{\mathrm{Ag}\,L_{\mathrm{II}}}$ (amps)	I_c (amps)	$B\varrho$ (gauss-cm)	E_{photo} (eV)
Ag $L_{\mathrm{III}\,(\mathrm{Cu}\,K\alpha_1)}$	129	2.98048	3.03722	227.191	4519.3
	130	2.97803	3.03463	227.198	4519.6
			Mean	227.195 ± 0.007	4519.5 ± 0.3

Ag L_{II}: B.E. + $\phi_{\mathrm{sp}} = 3528.0 \pm 0.6$ eV.

48. Cd

Table 15. Cd L_{III} (Cu $K\alpha_1$).

Calibration line	#	$I_{\mathrm{Cd}\,L_{\mathrm{III}}}$ (amps)	I_c (amps)	$B\varrho$ (gauss-cm)	E_{photo} (eV)
Cu A6	69	2.97357	3.72031	226.842	4505.6
	69	2.97370	3.72044	226.844	4505.6
	84	2.97311	3.71949	226.857	4506.1
	86	2.97300	3.71962	226.841	4505.5
			Mean	226.846 ± 0.004	4505.7 ± 0.2

Cd L_{III}: B.E. + $\phi_{\mathrm{sp}} = 3541.8 \pm 0.4$ eV.

49. In

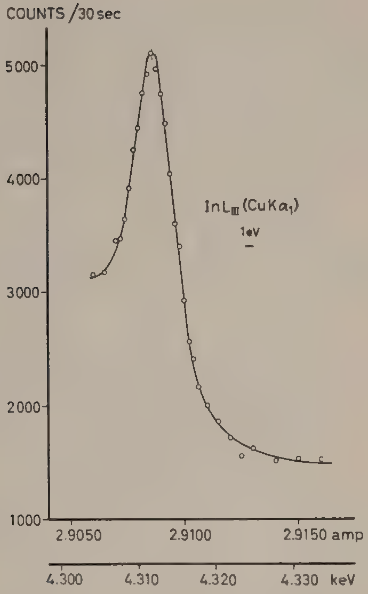

Fig. 18. InL_{III}(Cu$K\alpha_1$) photo line.

Table 16. In L_{III} (Cu $K\alpha_1$).

Calibration line	#	$I_{\text{In}L_{III}}$ (amps)	I_c (amps)	$B\varrho$ (gauss-cm)	E_{photo} (eV)
Cu A6	70	2.90865	3.71976	221.923	4313.1
	70	2.90850	3.71968	221.917	4312.8
	92	2.90894	3.72008	221.926	4313.2
	92	2.90902	3.72022	221.924	4313.1
			Mean	221.923 ± 0.004	4313.0 ± 0.2

In L_{III}: B.E. + $\phi_{sp} = 3734.5 \pm 0.4$ eV.

50. Sn

A study of energy shifts of the L levels in tin, due to oxidation, is given in reference (21). For one converter the L_I, L_{II} and L_{III} photo lines from metallic tin were all recorded in the same measurement (Fig. 19). This makes possible an energy determination of the L_I and L_{II} levels with respect to the L_{III} level. The data are listed in Tables 18 and 19.

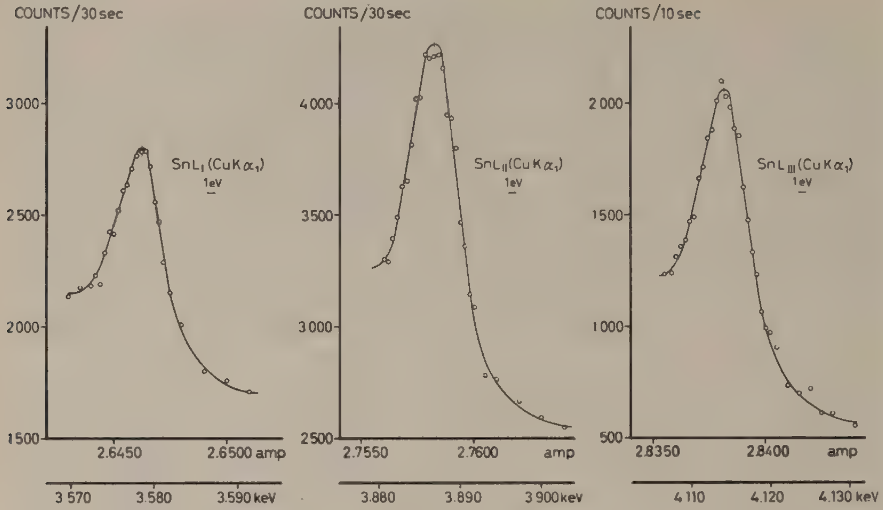

Fig. 19. SnL_I(Cu$K\alpha_1$), SnL_{II}(Cu$K\alpha_1$), and SnL_{III}(Cu$K\alpha_1$) photo lines.

Table 17. SnL_{III}(Cu$K\alpha_1$).

Calibration line	#	$I_{\mathrm{Sn}L_{\mathrm{III}}}$ (amps)	I_c (amps)	$B\varrho$ (gauss-cm)	E_{photo} (eV)
Cu A6	73	2.84052	3.71971	216.728	4114.3
	74	2.83978	3.71889	216.720	4114.0
	82	2.83848	3.71699	216.731	4114.4
	83	2.84078	3.72007	216.727	4114.2
			Mean	216.727 ± 0.004	4114.2 ± 0.2

Sn L_{III}: B.E. + $\phi_{sp} = 3933.3 \pm 0.4$ eV.

Table 18. SnL_{II}(Cu$K\alpha_1$).

Calibration line	#	$I_{\mathrm{Sn}L_{\mathrm{II}}}$ (amps)	I_c (amps)	$B\varrho$ (gauss-cm)	E_{photo} (eV)
SnL_{III}(Cu$K\alpha_1$)	113	2.75825	2.83811	210.630 ± 0.008	3886.8 ± 0.4

Sn L_{II}: B.E. + $\phi_{sp} = 4160.7 \pm 0.6$ eV.

Table 19. Sn L_{I}(Cu $K\alpha_1$).

Calibration line	#	$I_{\mathrm{Sn}L_{\mathrm{I}}}$ (amps)	I_c (amps)	$B\varrho$ (gauss-cm)	E_{photo} (eV)
Sn L_{III} (Cu Kα_1)	113	2.64622	2.83813	202.073 ± 0.008	3578.5 ± 0.4

Sn L_{I}: B.E. + $\phi = 4469.0 \pm 0.6$ eV.

51. Sb

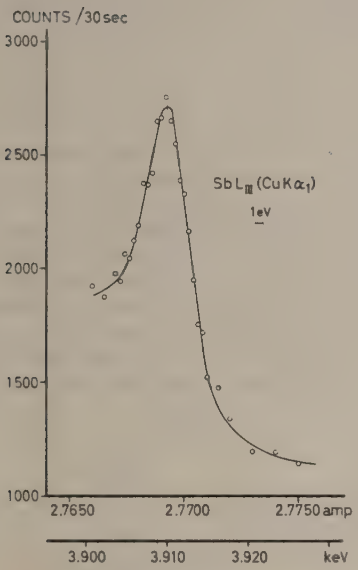

Fig. 20. SbL_{III}(Cu$K\alpha_1$) photo line.

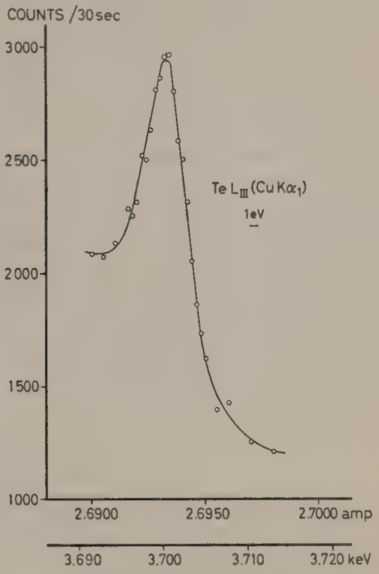

Fig. 21. TeL_{III}(Cu$K\alpha_1$) photo line.

Table 20. Sb L_{III}(Cu $K\alpha_1$).

Calibration line	#	$I_{\mathrm{Sb}L_{\mathrm{III}}}$ (amps)	I_c (amps)	$B\varrho$ (gauss-cm)	E_{photo} (eV)
Cu A6	71	2.76925	3.71995	211.277	3910.7
	71	2.76925	3.71986	211.282	3910.9
	89	2.76981	3.72059	211.283	3910.9
	89	2.76845	3.71878	211.282	3910.9
			Mean	211.281 ± 0.004	3910.8 ± 0.2

Sb L_{III}: B.E. + $\phi_{\mathrm{sp}} = 4136.7 \pm 0.4$. eV

52. Te

Table 21. Te L_{III} (Cu$K\alpha_1$).

Calibration line	#	$I_{\text{Te}L_{III}}$ (amps)	I_c (amps)	$B\varrho$ (gauss-cm)	E_{photo} (eV)
Cu A6	72	2.69329	3.71912	205.529	3701.5
	72	2.69348	3.71916	205.541	3702.0
	93	2.69348	3.71923	205.537	3701.8
	93	2.69344	3.71915	205.539	3701.9
			Mean	205.536 ± 0.004	3701.8 ± 0.2

Te L_{III}: B.E. + $\phi_{sp} = 4345.7 \pm 0.4$ eV.

4. *Work function correction*

To obtain the binding energy, B.E., as defined in section (I), one must correct for the work function, ϕ_{sp}, of the spectrometer material. The reproducibility of the measurements over a period of one year indicates that ϕ_{sp} remained constant. In order to determine ϕ_{sp}, an apparatus for measuring contact potentials by means of the Kelvin method was built. The principle is that of a vibrating condenser as described e.g., by Zisman (22). (This work was performed with E. Sokolowski, and a somewhat more detailed description is given in reference (6).) The contact potential between naturally aged copper and a freshly evaporated layer of silver was found to be 0.15 eV towards lower work function in copper. Subtracting this from the work function, 4.65 eV, of silver as measured by Hagström (23), one obtains for the work function of naturally aged copper (spectrometer material) the value:

$$\phi_{sp} = 4.5 \pm 0.3 \text{ eV}.$$

In Table 22 are listed the binding energies, B.E., obtained by subtracting the quantity ϕ_{sp} from the energy values given below Tables 6–21.

Table 22.

Shell	B.E. (eV)	Shell	B.E. (eV)
Cu K	8979.0	Ag L_{III}	3350.8
Cu L_{III}	931.7[1]	Ag L_{II}	3523.5
Zn K	9658.8	Cd L_{III}	3537.3
Ga K	10367.3	In L_{III}	3730.0
Ge K	11103.8	Sn L_{III}	3928.8
Ge L_I	1413.7	Sn L_{II}	4156.2
Se K	12657.7	Sn L_I	4464.5
		Sb L_{III}	4132.2
Rh L_{III}	3003.2	Te L_{III}	4341.2
Pd L_{III}	3172.9		

[1] See section (V).

V. Discussion of results

One of the earliest attempts to systematize experimental X-ray data was made by Moseley, who found that the $\sqrt{\nu/R}$ value of the same inner transition in various elements was an approximately linear function of the atomic number. If the square roots of the term values are plotted in the same way, a more irregular trend is observed (24). A further development was made with the introduction of the "modified" Moseley diagram. By subtracting a proper linear function from the $\sqrt{\nu/R}$ values, the energies can be examined in more detail (25). In a modified Moseley diagram the X-ray transition between two inner levels follows a parabolic curve. This is expected from the one-electron model, since with this model the function $\sqrt{\nu/R}$ contains higher powers of Z, and the coefficients are functions of the initial and final state quantum numbers. For a given transition these coefficients remain the same throughout the periodic system.

In a modified Moseley diagram of an absorption edge, i.e., of the binding energy of an inner atomic shell, the curvature due to higher order terms is obliterated by another phenomenon. The irregularities already seen in the original Moseley curves are magnified in the new scale diagram. This can be seen in Figs. 22 and 23. Here the binding energies obtained in the present investigation are plotted together with representative X-ray data. Discontinuities appear in the curves when an outer shell is completely filled. This is again to be expected from the one-electron theory of a *free atom*. Each time an outer shell is filled, the quantum numbers of the lowest unoccupied orbital are changed, and with free atoms the discontinuity should rather appear between the element which has a filled outer shell and the *preceding* element. However, it should be kept in mind that here we are dealing with atoms in the solid state and that the energies are related to the Fermi level of the crystal. If the level density is different in the bands and the overlapping not too great, a

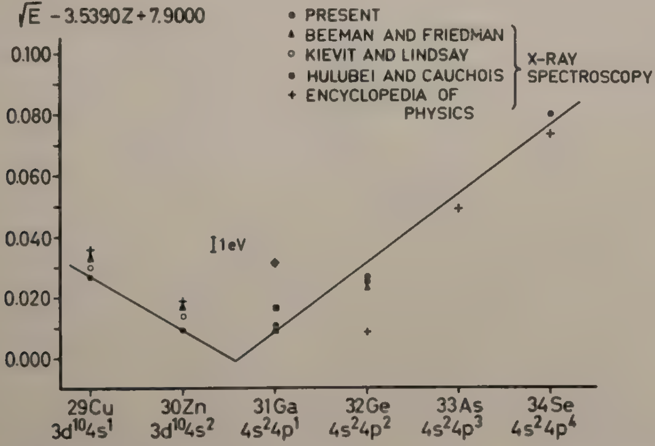

Fig. 22. Modified Moseley diagram for the K binding energies of the fourth period elements. X-ray data are taken from references (31), (30), (29), and (2). The electron configurations given refer to free atoms.

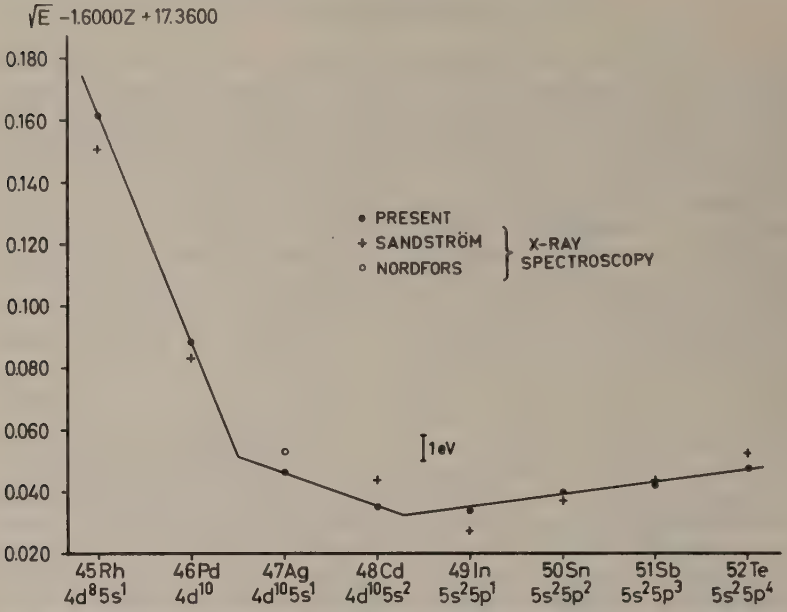

Fig. 23. Modified Moseley diagram for the L_{III} binding energies of the fifth period elements. X-ray data are taken from references (26) and (27).

discontinuity could be expected to occur *after* the element with a closed outer (sub)-shell. This is the case in Figs. 22 and 23, and hence the present results seem to be in accordance with band theory. It is believed that the precision of these measurements is high enough to make the discontinuities marked in the diagrams significant.

In principle, the binding energies obtained from X-ray absorption measurements should be the same as those determined by the photo electron method (cf. section I). For the elements rhodium through tellurium (except for silver) in the fifth period the wavelength values of the L_{III} absorption edges have been determined with a high degree of precision by Sandström (26). He estimates the errors in his wavelength values to be 0.5 x.u., which corresponds to about 0.5 eV. Nordfors has recently measured the L_{III} edge in silver with very high accuracy, after all precautions were taken to avoid impurities in the absorbers (27). His value for the AgL_{III} energy (plotted in Fig. 23) is 1.4 eV higher than that reported by Coster and Mulder (28), which they obtained directly from the silver bromide in a photographic emulsion.

Although the energy values determined by the photo electron method generally agree within experimental errors with those obtained with X-ray spectroscopy, some different trends are noticed in the diagrams (cf. also ref. (6)). In both periods the energies from photo electron measurements of the first two elements in the second row are approximately 1 eV lower than the energies obtained from absorption measurements, and for the elements indium through tellurium a different slope of the straight lines can be fitted to each sequence of energy values. A qualitative explanation of these discrepancies can be given in terms of the mechanism for X-ray

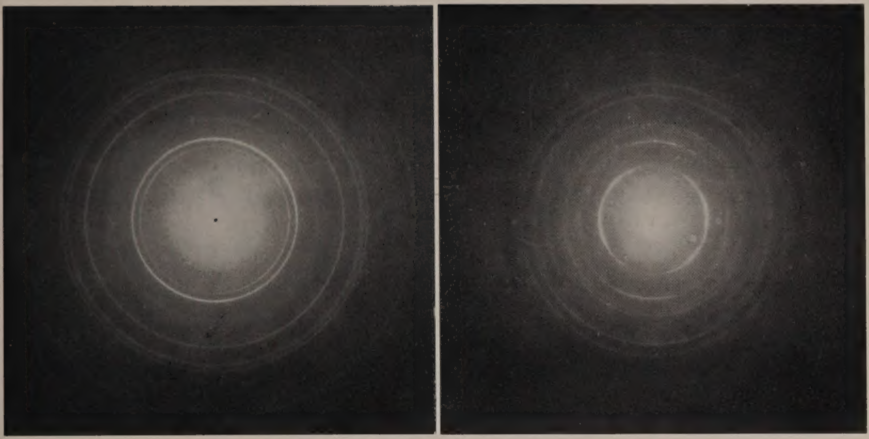

Fig. 24*a*. Fig. 24*b*.

Fig. 24. Electron diffraction patterns from thin metallic films of (a) zinc and (b) antimony. The antimony sample shows a high degree of orientation.

transitions discussed by Friedel (32), Landshoff (33), Parratt (34) and others. The vacancy in an inner electronic shell resulting from an absorption process is treated as a positive impurity in the lattice. Discrete "excitation states" are created that are characteristic of the impurity. The excess positive charge must be screened, and hence there is a reorganization of the valence electrons. Thus the absorption process is not a one-electron phenomenon, but several simultaneous electronic transitions are involved. The X-ray absorption edge is associated with the transition of lowest energy. However, it may be assumed that the energies in the conduction band of a metal are not changed considerably. The energies measured with the photo electron method are related to the Fermi level of the total crystal which is not influenced by the creation of this type of impurity states.

It was reported in reference (5) that oxidation of a metal may change the binding energies determined by the photo electron method. Also, for copper it was found that the K and L energies were not shifted by the same amount. From measurements of absorption edges and X-ray lines in metals and their oxides, Sanner concluded that, due to oxidation, no shift should be observed in the $K\alpha_1$ line of copper. However, until the present time no shift determinations have been published for this line. The shifts reported in reference (5) have been remeasured with an X-ray target of nickel, electroplated on a copper base, for the CuL_{III} shift measurements, and a molybdenum target for the K shift. These measurements confirmed the results obtained in the earlier investigation. To eliminate every possibility of disturbing effects from the slightly ferromagnetic nickel anode, the CuL_{III}(Cu$K\alpha_1$) photo line was also measured both with metallic copper and with CuO. The L_{III} shift obtained from this measurement also agreed with the earlier reported value within experimental errors. An energy calibration was made with the CuA6 line and the CuL_{III} binding energy in metallic copper (corrected for work function of spectrometer) was found to equal 931.7 eV. In Table 22 it is seen that the energy difference CuK–CuL_{III} is then 8047.3 eV as compared with 8047.5 eV for the Cu $K\alpha_1$ line; hence the X-ray transition energy for the metal can be obtained as the difference of two photo electron energies.

A further comparison of the data obtained in the present investigation with those determined by X-ray spectroscopy should be mentioned. The spin doublet separation of the L_{II} and L_{III} levels in silver and tin are 172.7 eV and 227.4 eV respectively, according to Table 22. Bergvall has recently remeasured the $K\alpha_1$ and $K\alpha_2$ lines in these elements (35), and found the energy difference between these lines to be 172.4 eV and 227.2 eV respectively.

Chemical shifts have been observed in the L shells for fifth period elements (21). In order to check the composition of the samples used in the present investigation, electron diffraction patterns were taken of sources prepared simultaneously with those used for the energy determinations, Fig. 24. The lattice constants obtained from the various patterns were compared with the data listed in the ASTM card catalogue (36) for the elements and their oxides. When precautions were taken to avoid unnecessary exposure to air, no oxidation could be detected in the films.

ACKNOWLEDGEMENTS

I wish to express my sincere gratitude to Professor Kai Siegbahn who initiated this investigation and whose never-failing interest in the work has been a great source of encouragement. I am much indebted to Fil. lic. Evelyn Sokolowski for help with the measurements and for many valuable discussions. My thanks are also due Fil. kand. Pär Bergvall for stimulating discussions, and Mr. William Parker for skillful assistance with source preparation and electron microscopy. The English manuscript has been revised by Mrs. Margie Hollander, who is thankfully acknowledged.

Institute of Physics, University of Uppsala.

REFERENCES

1. RICHTMYER, F. K., BARNES, S. W. and RAMBERG, E., Phys. Rev. *46*, 843 (1934).
2. SANDSTRÖM, A. E., in Encyclopedia of Physics XXX, 78, editor S. Flügge, Springer Verlag, Berlin (1955).
3. NILSSON, Å., Arkiv f. Fysik *6*, 513 (1953).
4. SOKOLOWSKI, E., NORDLING, C. and SIEGBAHN, K., Arkiv f. Fysik *12*, 301 (1957).
5. NORDLING, C., SOKOLOWSKI, E., and SIEGBAHN, K., Arkiv f. Fysik *13*, 483 (1958).
6. SOKOLOWSKI, E., Arkiv f. Fysik *15*, 1 (1959).
7. WEISSKOPF, V. and WIGNER, E., Zeits. f. Physik *63*, 54 (1930).
8. BEARDEN, J. A. and SHAW, C. H., Phys. Rev. *48*, 18 (1935).
9. MARTON, L., LEDER, L. B. and MENDLOWITZ, H., Advances in Electronics and Electron Phys. VII, 183 (1955).
10. PINES, D. and BOHM, D., Phys. Rev. *85*, 338 (1952).
11. PINES, D., in Solid State Physics, 1, editors F. Seitz and D. Turnbull, Acad. Press Inc., New York (1955).
12. KLEINN, W., Optik, *11*, 226 (1954).
13. MÖLLENSTEDT, G., Optik *5*, 499 (1949).
14. SIEGBAHN, K. and EDVARSON, K., Nucl. Phys. *1*, 137 (1956).
15. HARTREE, D. R., Proc. Camb. Phil. Soc. *21*, 746 (1923).
16. SIEGBAHN, K., Ark. Mat. Astr. Fys. *30 A*, 1 (1944).
17. BECKMAN, O., BERGVALL, P. and AXELSSON, B., Arkiv f. Fysik *14*, 419 (1958).
18. DU MOND, J. W. M. and COHEN, R. E., Rev. Mod. Phys. *25*, 691 (1953).

19. Gerholm, T. R., in Beta- and Gamma-Ray Spectroscopy, editor K. Siegbahn, North-Holland Publishing Co., Amsterdam (1955).
20. Sokolowski, E. and Nordling, C., Arkiv f. Fysik *14*, 557 (1959).
21. Nordling, C., Arkiv f. Fysik *15*, 241 (1959).
22. Zisman, W. A., Rev. Scient. Instr. *3*, 367 (1932).
23. Hagström, S., private communication.
24. Bohr, N. and Coster, D., Zeits. f. Physik *12*, 342 (1923).
25. Idei, S., Sci. Repts. Tôhoku Univ. *19*, 559 (1930).
26. Sandström, A. E., Nova Acta Reg. Soc. Sci. Upsal. No. 11 (1935).
27. Nordfors, B. To be published.
28. Coster, D. and Mulder, F. P., Zeits. f. Physik *38*, 264 (1926).
29. Hulubei, H. and Cauchois, Y., C. R. *211*, 316 (1940).
30. Kievit, B. and Lindsay, G. A., Phys. Rev. *36*, 648 (1930).
31. Beeman, W. W. and Friedman, H., Phys. Rev. *56*, 392 (1939).
32. Friedel, J., Phil. Mag. *43*, 153 (1952).
    —— Adv. in Phys. *3*, 446 (1954).
33. Landshoff, R., Phys. Rev. *55*, 631 (1939).
34. Parratt, L. G., Technical Report no. 8 AFOSR TN-56-562, ASTIA AD 110, 382. (ASTIA Document Service Center, Dayton 2, Ohio, USA (1958)).
35. Bergvall, P. To be published in Arkiv f. Fysik.
36. X-ray powder data file, published by the American Society for Testing Materials.

Tryckt den 24 april 1959

Uppsala 1959. Almqvist & Wiksells Boktryckeri AB